RSC Advances

PAPER

Cite this: *RSC Adv.*, 2024, **14**, 36084

Upconversion nanoparticles incorporated with three-dimensional graphene composites for electrochemical sensing of baicalin from natural plants†

Na Zhang,[abc] Yilin Wu,[b] Tian Liang,[b] Yongxiang Su,[b] Xusheng Xie,[b] Tianren Zhang,[b] Hongyan Wang,[b] Keying Zhang *[b] and Rongli Jiang*[a]

Chinese medicine has been widely studied owing to its many advantages. Baicalin (Bn), extracted from natural plants, has been shown to have significant anti-inflammatory and anticancer activity. Therefore, it is of great significance to develop a suitable method to detect the content of Bn in traditional Chinese medicine. Herein, we report an electrochemical sensor for the sensitive detection of Bn in *Scutellaria* root samples through a synergistic effect between upconversion nanoparticles (UCNPs) and three-dimensional macroporous graphene (3DG). The prepared UCNP-3DG composite was characterized using scanning electron microscopy (SEM), transmission electron microscopy (TEM) and X-ray diffraction spectroscopy (XRD). This proposed sensor exhibited a low detection limit of 3.8×10^{-8} M (S/N = 3). Importantly, the established method possesses good stability and selectivity and can successfully detect Bn in *Scutellaria* root samples. It provides a suitable strategy for the determination of Bn and has potential application prospects in the assay of traditional Chinese medicine.

Received 10th September 2024
Accepted 28th October 2024

DOI: 10.1039/d4ra06540a

rsc.li/rsc-advances

Introduction

Chinese medicine has been widely studied owing to its many advantages. Baicalin (Bn), a flavonoid, has remarkable anti-inflammatory and anticancer activity (Scheme 1). In addition, recent studies have proven that Bn has a series of biological effects, such as anti-allergy, clearing free radicals, inhibiting cancer cell proliferation, or inducing cell apoptosis.[1–5] Thus, it is significant to develop a reliable and sensitive method for assaying Bn derived from natural plants in the clinical and pharmaceutical fields. To date, a series of analysis methods, including thin-layer chromatography,[6] capillary electrophoresis,[7] high-performance liquid chromatography,[8] fluorescent[9,10] and photoluminescent[11] methods, liquid chromatography mass spectrometry,[12] and electrochemical methods,[13–20] have been designed to detect Bn. Among these methods, electrochemical strategies have great advantages in the analysis of Bn in actual samples owing to their excellent sensitivity, simple instrumentation, fast response speed, cost-effectiveness, and feasible miniaturization. The above merits make an electrochemical Bn sensor an attractive detection technology in the clinical and pharmaceutical fields.[21–25] Therefore, it is significant to exploit new electrochemical Bn sensors in the pharmaceutical analysis field.

Graphene, a carbon nanomaterial, exhibits a wide potential application in various fields[26–30] owing to its simple synthesis, low cost, multiple active sites, high electronic conductivity and excellent electrocatalytic activity. Additionally, graphene has been indicated to be a suitable promising material for constructing electrochemical sensors.[31–35] In recent years, three-dimensional graphene (3DG) has attracted considerable and widespread attention owing to its 3D porous structure, which

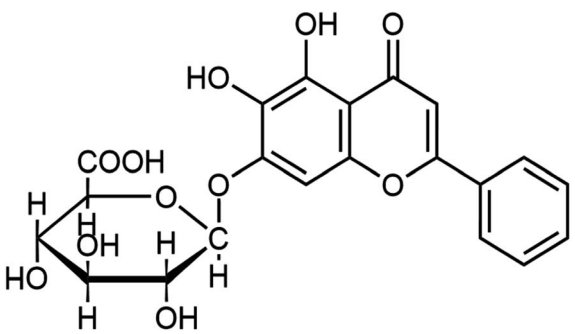

Scheme 1 Chemical structure of Bn.

[a]*School of Chemical Engineering and Technology, China University of Mining and Technology, Xuzhou, Jiangsu 221116, China. E-mail: ronglijcumt@163.com*

[b]*Anhui Key Laboratory of Spin Electron and Nanomaterials of Anhui Higher Education Institutes, School of Chemistry and Chemical Engineering, Suzhou University, Suzhou, Anhui, 234000, China. E-mail: zhangky1983@163.com*

[c]*Jiangsu Key Laboratory for Design and Manufacture of Micro-Nano Biomedical Instruments, Southeast University, Nanjing, Jiangsu 211189, China*

† Electronic supplementary information (ESI) available. See DOI: https://doi.org/10.1039/d4ra06540a

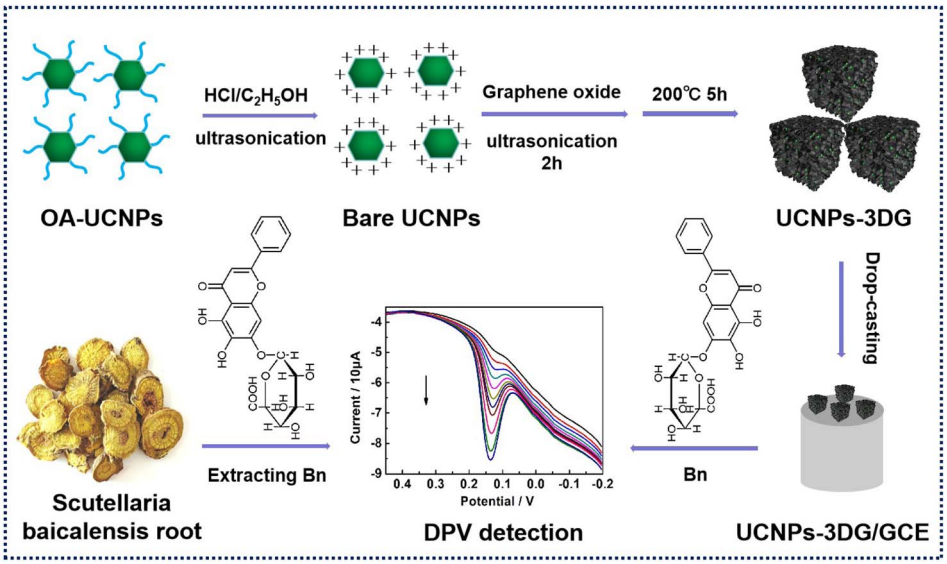

Scheme 2 Fabrication process of UCNP-3DG and its application in electrochemical detection of Bn in natural plant samples.

exhibits some merits such as adjustable internal space, large surface area, outstanding conductivity and good mechanical strength.[36–38] Therefore, it has been widely used in many fields, including electrochemical sensors and anode materials.[36–40] Recently, graphene oxide (GO) has been employed as a precursor for fabricating 3DG.[41] Remarkably, 3DG has been deeply investigated and successfully used as a good gelling agent to recombine other materials. In particular, the 3D porous structure of 3DG provides an opportunity to incorporate various types of materials, including polymers, nanoparticles and biomolecules, into 3DG to form hybrid materials.[41–44]

Upconversion nanoparticles (UCNPs) possess important application because of their merits, including special optical properties and good biocompatibility,[45] while their application in electrochemical sensor fields remains less explored. Previous reports[46,47] have revealed that bare rare earth ion-doped UCNPs have an abundant positive charge on their surfaces, which may provide a superior candidate for incorporating them into 3DG to form hybrid materials of UCNPs-3DG. In addition, bare UCNPs in hybrid materials may provide a platform that allows the enrichment of target molecules to improve the sensitivity of the electrochemical sensor.

Herein, an OA-UCNP ($NaYF_4$:Yb,Er) was fabricated and treated to obtain ligand-free UCNPs, which were then incorporated into 3DG to form a hybrid material (UCNPs-3DG). UCNPs-3DG, as a modifier, was coated onto the glass carbon electrode (GCE) surface to construct an electrochemical sensor allowing for sensitive detection of Bn in natural plants (Scheme 2), in which UCNP-3DG can amplify the detection signal by adsorbing abundant Bn to increase its concentration on the modified electrode surface. Meanwhile, the active sites of 3DG provide the capability to accelerate the redox of Bn on the UCNP-3DG/GCE surface. Thus, using the synergistic effects of 3DG and UCNPs, the final electrode displays better performance in detecting Bn. This may provide a candidate for the analysis of Bn in actual samples.

Materials and methods

Preparation of 3DG and UCNPs-3DG

The OA-UCNPs (OA-$NaYF_4$:Yb,Er) were prepared and then transferred into water according to a previous report.[46] The process is shown in the ESI.† Referring to the previous literature to fabricate 3DG and UCNP-3DG,[41] 3DG was fabricated by transferring 10 mL of GO (2.5 mg mL^{-1}) into a reactor at 200 °C for 5 h. The solid powder of 3DG was then collected by applying the freeze drying method. UCNP-3DG was synthesized by adding 50 mg of ligand-free UCNPs into 10 mL 2.5 mg per mL GO solution for maintaining continuous ultrasound for 2 h. After that, the suspension was transferred into a reactor at 200 °C for 5 h. Finally, the solid powder of UCNP-3DG was collected by applying the freeze drying method.

Preparation of UCNPs-3DG/GCE

Before modification, bare GCE was carefully sequentially polished by 1.0, 0.3 and 0.05 μm alumina powder suspension. Then, the treated GCE was orderly and ultrasonically cleaned using ethanol and double-distilled water for 1.0 min.

10.0 mg UCNP-3DG was dispersed in 10 mL *N*,*N*-dimethylformamide through ultrasonic method keeping for 30 min to form the suspension of UCNPs-3DG. 10 μL UCNP-3DG suspension was then dropped onto the cleaned GCE surface and allowed for drying at room temperature. After that, the loosely adsorbed UCNP-3DG on the electrode surface was removed by immersing it in water for 10 min and washing it three times with water. Finally, The UCNP-3DG/GCE was successfully prepared.

Results and discussion

Compositional and morphological features of UCNPs-3DG

SEM was employed to investigate the morphology and microstructures of UCNPs-3DG. Fig. 1A displays the typical SEM

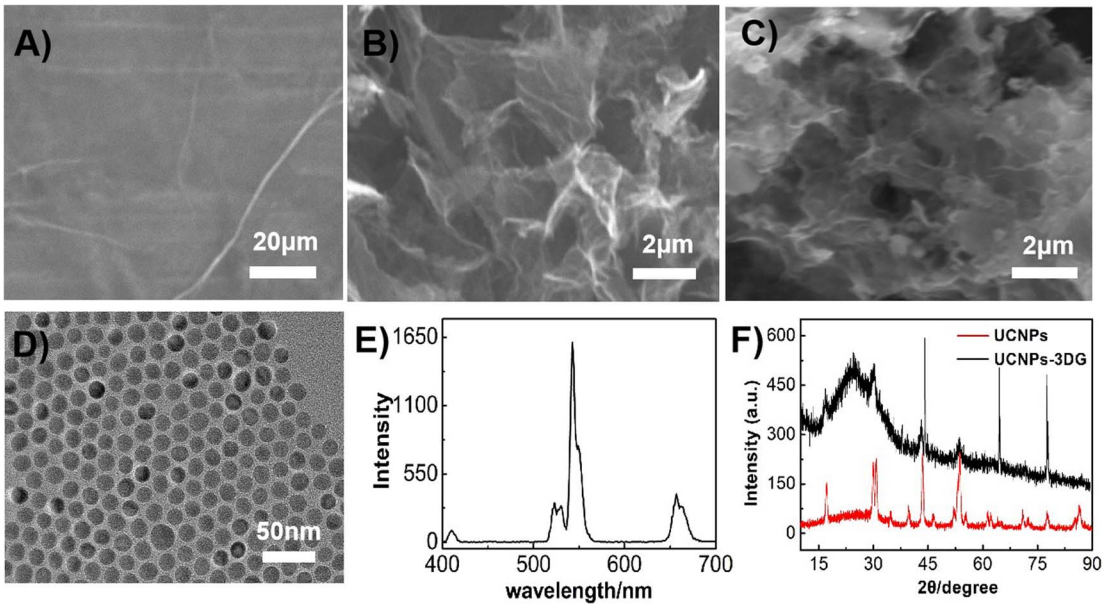

Fig. 1 SEM images of GO (A), 3DG (B) and UCNP-3DG (C). TEM image of UCNPs (D). Luminescence of UCNPs with a 980 nm laser as the excitation light source (E). XRD spectra of UCNPs and UCNP-3DG (F).

morphology of GO. After the treatment, GO was turned into an interconnected 3D framework and exhibited a "sporelike" structure (Fig. 1B), which was similar to the previous report.[41] This structure can provide a larger surface area and large enough space for Bn to penetrate into the interior spaces and material surface, resulting in a high concentration of Bn on the electrode surface. Fig. 1C shows that UCNP-3DG possesses more "sporelike" structures compared with Fig. 1B. The TEM image displayed that UCNPs had uniform morphology with a size of ≈17.0 nm (Fig. 1D), and the typical green luminescence of UCNPs was found under a 980 nm laser excitation (Fig. 1E). XRD was employed to further verify the formation of UCNP-3DG (Fig. 1F). These well-preserved UCNPs are expected to provide a platform for the enrichment of Bn. The 3DG accelerates the electron transfer during the process of the redox of Bn at the UCNP-3DG/GCE surface.

CV response of Bn

The CV responses of Bn at the various electrode surfaces were investigated in 0.1 M PBS (pH = 7.0). As shown in Fig. 2A, the CV curves of Bn at the different electrodes, including bare GCE (a), UCNPs/GCE (b), 3DG/GCE (c) and UCNPs-3DG/GCE (d), were recorded. The above several materials can maintain stability on the GCE surface owing to the adsorption effect. A weak electrochemical response of Bn was observed at bare GCE (a), and a higher CV response of Bn was observed on the UCNPs/GCE surface (b), which confirmed that the electrochemical process of Bn that occurred on the UCNPs/GCE surface was enhanced.

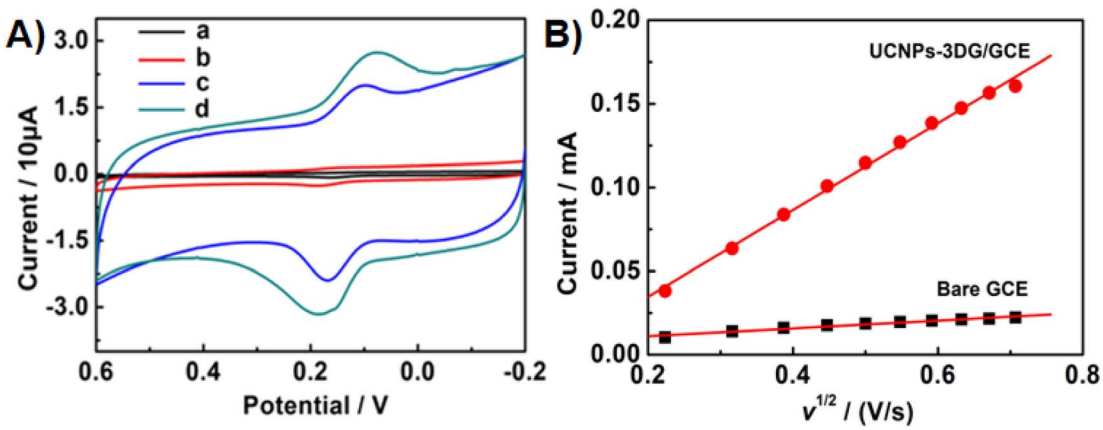

Fig. 2 (A) CVs of Bn at different electrode surfaces: bare GCE (a), UCNPs/GCE (b), 3DG/GCE (c) and UCNPs-3DG/GCE (d) in 0.1 M PBS (pH = 7.0). Scan rate: 0.1 V s^{-1}. (B) Relationship between the anodic peak current and the square root of the scan rate for different electrodes in 0.1 M KCl solution containing 1.0 mM $K_3Fe(CN)_6$.

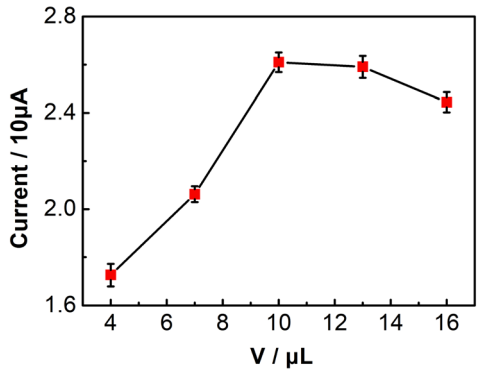

Fig. 3 Amounts of UCNP-3DG *vs.* the oxidation peak current of Bn.

Compared to the bare GCE and UCNP modified electrode, 3DG/GCE displayed large background currents and good catalytic performance for Bn. Additionally, differential pulse voltammetry (DPV) was employed to investigate the electrochemical behavior of Bn on various electrode surfaces. The results are shown in Fig. S1.† The highest peak current of Bn was observed for UCNPs-3DG/GCE. The above results were owing to the good conductivity and large surface area of UCNPs-3DG. More importantly, the UCNPs-3DG/GCE exhibited a better electrocatalytic ability for the redox of Bn (d) using the synergistic effect of UCNPs and 3DG. Thus, UCNPs can amplify the detection signal by adsorbing abundant Bn to increase its concentration on the electrode surface, and the active sites of 3DG can hasten the electron transfer during the process of the redox of Bn on the UCNP-3DG/GCE surface.

The Randles–Sevcik equation was used to calculate the active area of the UCNPs-3DG/GCE by CV in 0.1 M KCl containing 1.0 mM $K_3Fe(CN)_6$.[48] A reversible process equation ($T = 298$ K) is as follows:

$$I_p = (2.69 \times 10^5) n^{3/2} A D_0^{1/2} \nu^{1/2} C_0^*, \quad (1)$$

where I_p represents the anodic peak current, n represents the electron transfer number (=1), A represents the electrode surface area, D_0 is the diffusion coefficient (7.6×10^{-6} cm^2 s^{-1}), ν is scan rate, and C_0^* is the concentration of $K_3Fe(CN)_6$. The electrode active area (A) can be calculated by the slope of the plot of I_p *vs.* $\nu^{1/2}$. As shown in Fig. 2B, the slopes were 0.02348 and 0.2593 for bare GCE and the UCNPs-3DG/GCE, respectively. Based on eqn (1), A was calculated to be about 0.03 cm^2 and 0.34 cm^2, respectively.

Optimization of the amount of UCNPs-3DG

The amount of UCNP-3DG on the GCE surface is a key effect factor for the performance of UCNPs-3DG/GCE for determining Bn. Therefore, we selected different amounts of UCNP-3DG to fabricate the modified electrode ($c_{\text{UCNP-3DG}} = 1.0$ mg mL^{-1}; 4.0, 7.0, 10.0, 13.0, and 16.0 μL), and the amount of UCNP-3DG was optimized by employing the oxidation peak current of Bn as a signal *via* CV in 0.1 M PBS (pH = 7.0) under a scan rate of 0.1 V s^{-1}. As shown in Fig. 3, when 10.0 μL of UCNP-3DG suspension was modified onto the surface of the electrode, the oxidation peak current of Bn reached its maximum value. This may be attributed to the significant thickness of the modified film formed by the superfluous UCNPs-3DG, hindering electron transfer. Thus, 10.0 μL (1.0 mg mL^{-1}) of UCNP-3DG suspension was chosen as the optimal amount to construct the UCNPs-3DG/GCE.

Optimization of accumulation time

The accumulation time of Bn on UCNPs-3DG/GCE is an important factor affecting the performance of the proposed sensor. Under static conditions, the effect of accumulation time was studied using DPV 0.1 M PBS (pH = 7.0) containing 5.0×10^{-6} M Bn. As shown in Fig. 4, the oxidation peak current increased as the accumulation time increased in the range from 0 to 24 min and then reached a plateau until 15 min, indicating that the accumulation amount of Bn on the electrode surface had reached saturation. Therefore, 15 min was selected as the optimization accumulation time.

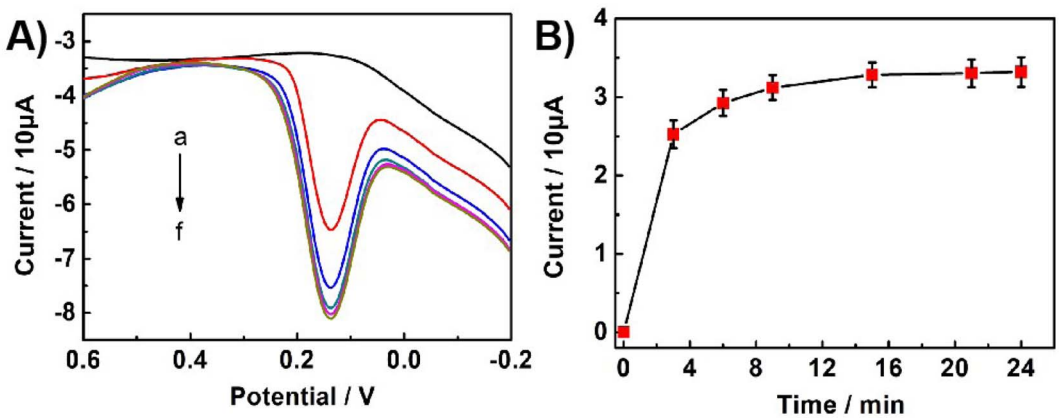

Fig. 4 (A) DPVs of Bn at the UCNPs-3DG/GCE at different accumulation times in 0.1 M PBS (pH = 7.0). The concentration of Bn: 5.0×10^{-6} mol L^{-1}. (B) The oxidation peak current of Bn *vs.* the accumulation time: (a) 0 min, (b) 3.0 min, (c) 9.0 min, (d) 15.0 min, (e) 21.0 min, and (f) 24.0 min.

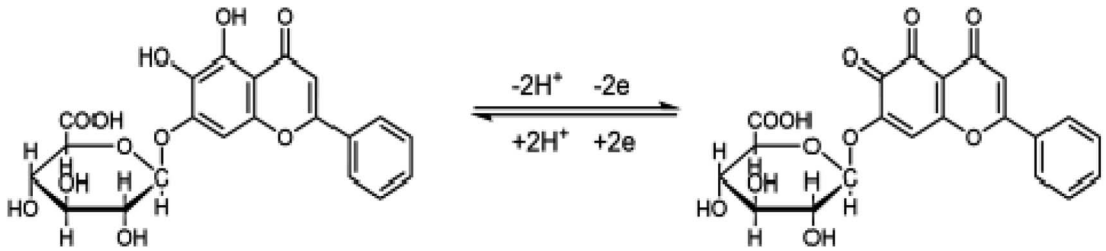

Scheme 3 Electrochemical redox mechanism of Bn.

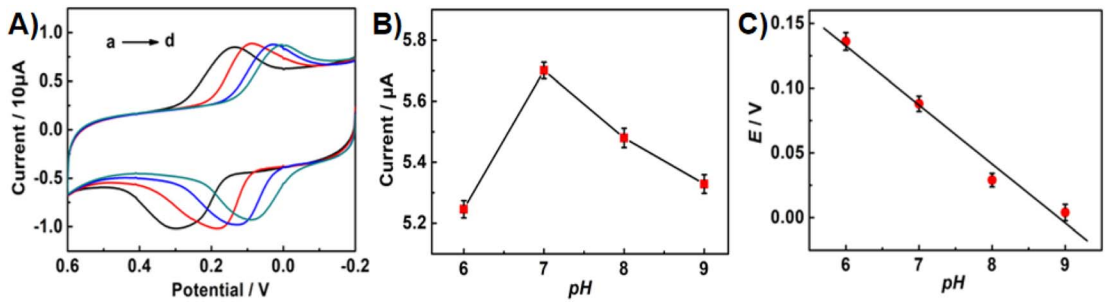

Fig. 5 (A) CVs of Bn on UCNPs-3DG/GCE in 0.1 M PBS at different pH values. (B) Oxidation peak current of Bn *vs.* pH. (C) Oxidation peak potential of Bn *vs.* pH. (a) 6.0, (b) 7.0, (c) 8.0, and (d) 9.0. Scan rate: 0.1 V s^{-1}.

Influence of pH

CV was employed to investigate the effect of pH value on the electrochemical behaviours of Bn on the UCNPs-3DG/GCE in 0.1 M PBS with various pH values. As depicted in Fig. 5A, higher redox peak currents of Bn were observed at pH 7.0 (Fig. 5B). Thus, pH 7.0 was selected as the optimal pH value in the subsequent experiments. Meanwhile, Fig. 5C shows that the Bn redox peak potential shifted negatively as the pH value increased, and the reduction peak potential displayed a desirous linear relationship with the pH value ($E_{pa} = -0.0455\text{pH} + 0.4055$, $R^2 = 0.9889$).

According to the Nernst equation, $dE_p/d\text{pH} = 2.303mRT/nF$, $m/n \approx 0.78$ was calculated, indicating that the values of m and n were identical in the redox process of Bn on UCNPs-3DG/GCE. Additionally, the slope of 0.0455 basically meets the requirement of the theoretical value (55 mV pH^{-1}). According to previous reports,[21–23] the redox process of Bn is an equal electron-equal proton transfer process. The electrochemical redox mechanism of Bn is shown in Scheme 3.

Influence of scan rate

Fig. 6A displays the CVs of Bn at the UCNPs-3DG/GCE under the different scan rates. The redox peak current was linearized with a scan rate in the range of 20–200 mV s^{-1} ($i_{pa} = 0.0289\nu$ (mV s^{-1}) − 0.379, $R^2 = 0.9935$; and $i_{pc} = -0.0255\nu$ (mV s^{-1}) − 0.3998, $R^2 = 0.9971$). The experimental results demonstrate that the redox process of Bn on the UCNP-3DG/GCE surface is governed by adsorption.

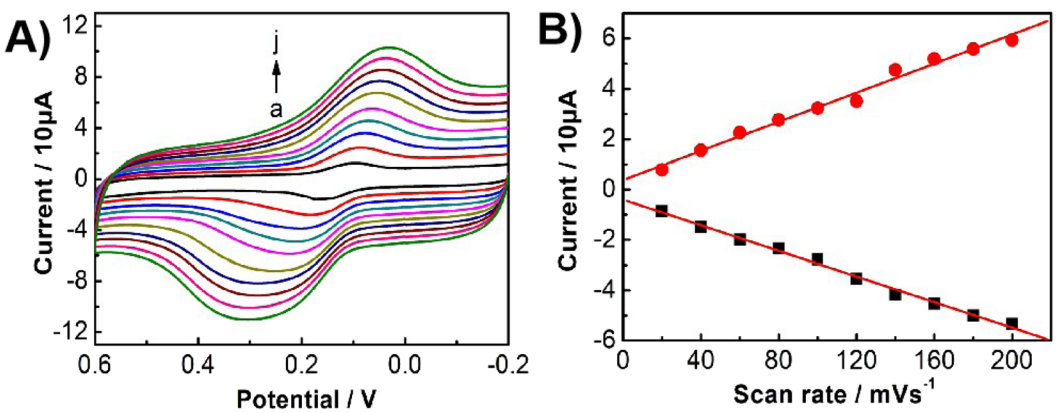

Fig. 6 (A) CVs of Bn on UCNPs-3DG/GCE in 0.1 M PBS under different scan rates in 0.1 M PBS (pH 7.0). (B) Redox peak current of Bn *vs.* scan rate. (a) 20 mV s^{-1}, (b) 40 mV s^{-1}, (c) 60 mV s^{-1}, (d) 80 mV s^{-1}, (e) 100 mV s^{-1}, (f) 120 mV s^{-1}, (g) 140 mV s^{-1}, (h) 160 mV s^{-1}, (i) 180 mV s^{-1}, and (j) 200 mV s^{-1}.

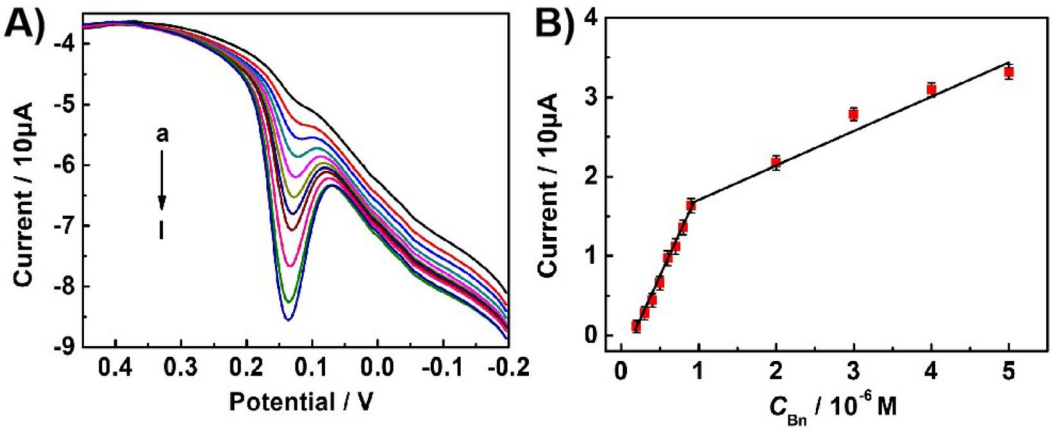

Fig. 7 (A) DPVs of different concentrations of Bn on the UCNPs-3DG/GCE in 0.1 mol per L PBS (pH = 7.0). (B) Oxidation peak current of Bn *vs.* concentration. (a) 2.0×10^{-7} M, (b) 3.0×10^{-7} M, (c) 4.0×10^{-7} M, (d) 5.0×10^{-7} M, (e) 6.0×10^{-7} M, (f) 7.0×10^{-7} M, (g) 8.0×10^{-7} M, (h) 9.0×10^{-7} M, (i) 2.0×10^{-6} M, (j) 3.0×10^{-6} M, (k) 4.0×10^{-6} M, and (l) 5.0×10^{-6} M.

Sensitivity of the sensor

The sensitivity of the constructed electrochemical sensor for Bn was evaluated by recording the DPV response of the oxidation peak of Bn in 0.1 M PBS (pH 7.0) under optimal experimental conditions. Fig. 7A displays the typical DPV response curves with different concentrations of Bn on the UCNPs-3DG/GCE. The oxidation peak current of Bn linearized with its concentration ranges from 2.0×10^{-7} to 9.0×10^{-7} M and 9.0×10^{-7} to 5.0×10^{-6} M. The linear regression equations i_p (10 μA) = 2.19c (M) − 0.38 (R^2 = 0.9968) and i_p (10 μA) = 0.42c (M) + 1.34 (R^2 = 0.9842) were obtained (Fig. 7B) The limit of detection reached 3.8×10^{-8} M (signal/noise = 3), which had better performances of linear wide and detection limit than previously reported methods.[10,16,49,50] The results are shown in Table 1. The improved performance may have resulted from the synergistic effect between UCNPs and 3DG. Moreover, UCNPs can amplify the detection signal by adsorbing abundant Bn to increase its concentration on the UCNP-3DG/GCE surface, and the active sites of the 3DG hasten the electron transfer during the process of the redox of Bn on the UCNPs-3DG/GCE.

Repeatability, reproducibility, and stability of the sensor

The repeatable ability of the constructed sensor was evaluated by employing it to detect 1.0×10^{-6} M Bn eight times. As shown in Fig. 8A, the relative standard deviation (R.S.D.) of about 4.1% was obtained for the oxidation currents of Bn, indicating that the established sensor was of good repeatability.

The reproducible ability of the constructed sensor was studied by independently fabricating five UCNP-3DG/GCE to detect 1.0×10^{-6} M Bn. The DPV response of the different electrodes is shown in Fig. S2.† Fig. 8B displays that the R.S.D. was 2.8%, which demonstrated that the proposed sensor was of excellent reproducibility.

The stability of the modified electrode was also researched by CV scanning for 30 cycles. After that, the UCNP-3DG/GCE was placed in 0.1 M PBS (pH 7.0) for 7 d at 4 °C. The treated electrode was then employed to determine Bn at the same concentration. About 96% of the initial peak currents remained, indicating that the proposed electrode was of excellent stability.

Selectivity of the constructed sensor

The anti-interference capability of the UCNPs-3DG/GCE was tested by detecting 2.0×10^{-6} M Bn in 0.1 M PBS (pH 7.0) with various potential interfering substances, including Zn^{2+}, Mg^{2+}, sucrose (Suc), glucose (Glu), L-cysteine (L-cys), and ellagic acid (Ea), by DPV to study the selectivity of the established sensor. The test results displayed that 100 times the interfering substances of the target analyte barely affected the determination of Bn (Fig. 9). This demonstrates that the proposed method

Table 1 Performance of the proposed method using some previous methods

Modified electrode	Methods	Linear range (10^{-6} M)	Detection limit (10^{-9} M)	Ref.
N, S co-doped carbon dots	Fluorescent	0.69–70.0	210.0	10
MoS_2/CILE	DPV	0.125–12.5	50.0	16
PT-NCDS	Fluorescent	0.1–20.0	43.8	49
Boron-doped diamond	SWV	0.95–1.0	260.0	50
UCNPs-3DG/GCE	DPV	0.2–0.9 0.9–5.0	38.0	This work

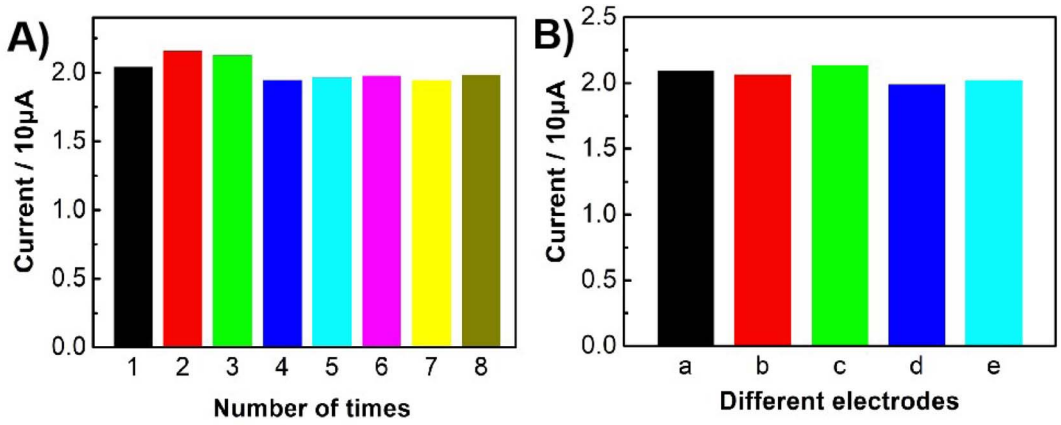

Fig. 8 (A) DPV response of the proposed sensor to the same concentration of Bn. (B) DPV responses of UCNPs-3DG/GCE independently prepared under the same conditions to the same concentration of Bn. $c_{Bn} = 1.0 \times 10^{-6}$ M.

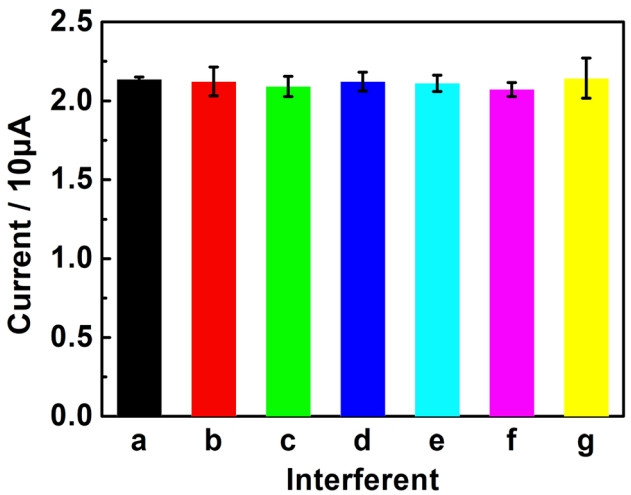

Fig. 9 DPV responses of the UCNPs-3DG/GCE to Bn in the presence of various interfering substances. (a) No interfering substance, (b) Zn^{2+}, (c) Mg^{2+}, (d) Suc, (e) Glu, (f) L-cys, and (g) Ea. $c_{Bn} = 2.0 \times 10^{-6}$ M.

has excellent selectivity. This may have great application prospects in the detection of Bn in actual samples.

Detecting real samples

The application ability of this constructed method was first evaluated by using it to detect Bn in the *Scutellaria* root. The treatment method of natural plant samples is according to previous reports.[25] Briefly, the natural plant extracts were obtained by putting 60.0 g *Scutellaria* baicalensis root into 15 mL of ethanol, refluxed under 50 °C and kept for 4 h. After that, 0.1 M PBS (pH 7.0) was used to dilute the obtained extracts. The standard addition method was adopted. The oxidation current of each sample was recorded and then plugged into the standard curve equation to calculate the concentration of Bn. As shown in Table 2, the UCNP-3DG/GCE exhibited satisfactory detection performances of the *Scutellaria* root samples with a recovery of 95.3–101.6%, indicating that the constructed sensor can be used to analyze Bn in real samples. The modified electrode has great potential application prospects in the detection of Bn in actual samples.

Table 2 Determination results of Bn in real samples ($n = 3$)

No.	Added (10^{-7} M)	Found (10^{-7} M)	Recovery (%)
1	0	2.5	—
2	3.0	5.3	96.4
3	6.0	8.1	95.3
4	10.0	12.7	101.6

Conclusions

Herein, a Bn electrochemical sensor based on UCNPs-3DG/GCE was constructed, which displayed excellent performance in the redox of Bn. The synergistic effect of UCNPs and 3DG can amplify the detection signal by adsorbing abundant Bn and hasten the electron transfer during the process of the redox of Bn at the UCNP-3DG/GCE surface, allowing for highly sensitive detection of Bn with a detection limit of 3.8×10^{-8} M. Additionally, the established method displayed a wide linear range, excellent repeatability, remarkable reproducibility and long-term stability. More importantly, it can be successfully applied to determine Bn in natural plants, which implies that the developed method has great potential application prospects in the fields of food and medicine.

Data availability

All data generated or analysed during this study are included in this published article and its ESI.†

Author contributions

Na Zhang: conceptualization, supervision, writing – original draft, funding acquisition. Yilin Wu: visualization. Yongxiang Su: conceptualization. Xusheng Xie: visualization. Tian Liang:

visualization. Hongyan Wang: funding acquisition. Rongli Jiang: visualization, writing – review & editing. Keying Zhang: writing – review & editing, funding acquisition.

Conflicts of interest

The authors declare no competing interests.

Acknowledgements

This work was supported by the Natural Science Foundation of Anhui Province (2108085MB67), the Open Research Fund of Jiangsu Key Laboratory for Design and Manufacture of Micro-Nano Biomedical Instruments, Southeast University (KF202302), the Academic Funding Project for Top Talents in Disciplines of Anhui Universities (DTR2023054), the Project of Anhui Province Excellent Research and Innovation Team (2024AH010029), the Natural Science Research Key Project of Education Department of Anhui Province (2023AH040315). The Suzhou University Development Fund and Research Platform (2021XJPT06, 2020XJSN01, 2020XJXS03) the Horizontal Subject (2023xhx295).

References

1 X. Y. Lu, W. He, W. L. Yang, J. L. Li, W. Q. Han, Q. Liu, T. Zhang, J. W. Jiang, A. Qin and Q. Yu, *J. Cell. Mol. Med.*, 2018, **22**, 5029–5039.
2 B. Dinda, S. Dinda, S. D. Sharma, R. Banik, A. Chakraborty and M. Dinda, *Eur. J. Med. Chem.*, 2017, **131**, 68–80.
3 S. Singh, A. Meena and S. Luqman, *Pharmacol. Res.*, 2021, **164**, 105387.
4 M. A. Ozma, E. Khodadadi, F. Pakdel, F. S. Kamounah, M. Yousefi, B. Yousefi, M. Asgharzadeh, K. Ganbarov and H. S. Kafil, Baicalin, *J. Herb. Med.*, 2021, **27**, 100432.
5 T. Huang, Y. Liu and C. Zhang, *Eur. J. Drug Metab. Pharmacokinet.*, 2019, **44**, 159–168.
6 M. Okamoto, M. Ohta, H. Kakamu and T. Omori, *Chromatographia*, 1993, **35**, 281–284.
7 G. Chen, H. Zhang and J. Ye, *Talanta*, 2000, **53**, 471–479.
8 S. Liu, L. Zhao, X. Liu, F. Zhou and S. Jiang, *J. Food Drug Anal.*, 2004, **12**, 306–310.
9 W. Jiang, H. Jin, Y. J. Sun, Z. J. Sun and R. J. Gui, *Biosens. Bioelectron.*, 2020, **152**, 112012.
10 J. Zhang, D. Y. Nan, S. Pan, H. Liu, H. Yang and X. L. Hu, *Spectrochim. Acta, Part A*, 2019, **221**, 117161.
11 K. Y. Huang, X. Huang, X. Y. Fang, S. Cheng, W. M. Sun, H. A. A. Noreldeen, Q. Zhang, H. H. Deng and W. Chen, *Sens. Actuators, B*, 2022, **368**, 132197.
12 J. Feng, W. Xu, X. Tao, H. Wei, F. Cai, B. Jiang and W. Chen, *J. Pharm. Biomed. Anal.*, 2010, **53**, 591–598.
13 M. T. Zhang, X. J. Huang, J. J. Li, Y. H. Li, P. C. Zhao, J. J. Fei and Y. X. Xie, *Colloids Surf., A*, 2023, **669**, 131484.
14 L. Zhang, J. J. Li, P. C. Zhao, C. X. Wang, Y. L. Wang, Y. Q. Yang, Y. X. Xie and J. J. Fei, *Microchem. J.*, 2022, **182**, 107873.
15 C. Monteiro, J. P. Winiarski, E. R. Santana, B. Szpoganicz and I. C. Vieira, *Materials*, 2023, **16**, 1024.
16 Y. Zhang, T. Y. Wang, Y. L. Qiu, F. F. Fu and Y. Y. Yu, *J. Electroanal. Chem.*, 2016, **775**, 286–291.
17 W. B. Hu, W. Zhang, M. Wang and F. Hu, *J. Electron. Mater.*, 2018, **47**, 1151–1157.
18 K. Sheng, L. Wang, H. C. Li and B. X. Ye, *Talanta*, 2017, **164**, 249–256.
19 Y. J. Guo and C. Dong, *Biosens. Bioelectron.*, 2014, **58**, 242–248.
20 L. M. Rao, P. C. Zhou, P. Liu, X. Y. Lu, X. M. Duan, Y. P. Wen, Y. F. Zhu and J. K. Xu, *J. Electroanal. Chem.*, 2021, **898**, 115591.
21 W. J. Jiang, S. Y. Wu, G. R. Fan, Z. D. Wang, S. X. Chen, Y. P. Wen and P. Wang, *New J. Chem.*, 2022, **46**, 16341–16351.
22 B. Kong, X. Yang, H. Q. Dai, Y. Wu, H. B. Lu, W. Liu and X. Y. Liu, *Electroanalysis*, 2022, **34**, 1564–1571.
23 P. C. Zhao, L. Z. Huang, H. Wang, C. X. Wang, J. Chen, P. P. Yang, M. J. Ni, C. Chen, C. Y. Li, Y. X. Xie and J. J. Fei, *Sens. Actuators, B*, 2022, **350**, 130853.
24 Y. L. Gao, W. Y. Pang, X. L. Chang, Z. Y. Hu, T. P. Hu and X. M. Ma, *J. Solid State Electrochem.*, 2024, **28**, 2959–2971.
25 J. Li, Y. F. Wang, C. X. Wang, Y. L. Wang, Y. Q. Yang, J. Chen, C. Y. Li, Y. X. Xie, P. C. Zhao and J. J. Fei, *Carbon*, 2023, **202**, 125–136.
26 J. Y. Wu, H. Lin, D. J. Moss, K. P. Loh and B. H. Jia, *Nat. Rev. Chem*, 2023, **7**, 162–183.
27 H. M. Wang, H. S. Wang, C. X. Ma, L. X. Chen, C. X. Jiang, C. Chen, X. M. Xie, A. P. Li and X. R. Wang, *Nat. Rev. Phys.*, 2021, **3**, 791–802.
28 T. Liu, Y. Yang, S. W. Cao, R. H. Xiang, L. Y. Zhang and J. G. Yu, *Adv. Mater.*, 2023, **35**, 2207752.
29 M. H. Wang, M. Huang, D. Luo, Y. Q. Li, M. Choe, W. K. Seong, M. Kim, S. Jin, M. R. Wang, S. Chatterjee, Y. Kwon, Z. Lee and R. S. Ruoff, *Nature*, 2021, **596**, 519–524.
30 R. G. Ma, Y. Zhou, H. Bi, M. H. Yang, J. C. Wang, Q. Liu and Fu. Q. Huang, *Prog. Mater. Sci.*, 2020, **113**, 100665.
31 B. B. Zhou, H. Xie, S. S. Zhou, X. X. Sheng, L. Chen and M. Zhong, *Food Chem.*, 2023, **423**, 136294.
32 A. A. Lahcen, S. Rauf, T. Beduk, C. Durmus, A. Aljedaibi, S. Timur, H. N. Alshareef, A. Amine, O. S. Wolfbeis and K. N. Salama, *Biosens. Bioelectron.*, 2020, **168**, 112565.
33 B. J. Sanghavi, S. Sitaula, M. H. Griep, S. P. Karna, M. F. Ali and N. S. Swami, *Anal. Chem.*, 2013, **85**, 8158–8165.
34 A. A. Sabbaghi, H. Dastangoo and K. Asadpour-Zeynali, *Talanta*, 2023, **253**, 123928.
35 J. N. Yao, Y. Huang, Y. Hou, B. Yang, L. C. Lei, X. J. Tang, K. G. Scheckel, Z. J. Li, D. Wu and D. D. Dionysiou, *Chem. Eng. J.*, 2021, **405**, 126545.
36 Z. X. Sun, S. Y. Fang and Y. H. Hu, *Chem. Rev.*, 2020, **120**, 10336–10453.
37 N. Baig, A. Waheed, M. Sajid, I. Khan, A. N. Kawde and M. Sohail, *Trends Environ. Anal. Chem.*, 2021, **30**, e00120.
38 V. K. R. Kondapalli, O. I. Akinboye, Y. Zhang, G. Donadey, J. Morrow, K. Brittingham, A. A. Raut, M. Khosravifar, B. Al-Riyami, J. H. Bahk and V. Shanov, *ACS Appl. Mater. Interfaces*, 2024, **16**, 13150–13160.

39 I. Johnson, J. H. Han and M. W. Chen, *Acc. Mater. Res.*, 2022, **3**, 1011–1021.
40 H. T. Wang, X. Y. Mi, Y. Li and S. H. Zhan, *Adv. Mater.*, 2020, **32**, 1806843.
41 R. B. Song, S. Zhou, D. Guo, P. P. Li, L. P. Jiang, J. R. Zhang, X. G. Wu and J. J. Zhu, *ACS Sustainable Chem. Eng.*, 2020, **8**, 1311–1318.
42 E. J. Lee, Y. M. Kwon, G. Bae, S. Y. Park, D. S. Song, H. K. Jo, D. H. Lee, H. Y. Jeon, S. Kang, S. Yim, S. Myung, J. Lim, S. S. Lee, D. H. Yoon and W. Song, *Adv. Mater. Interfaces*, 2024, **11**, 2400041.
43 W. W. Huan, B. Liu, P. H. Liu, F. Gao, Y. M. Zhang, L. M. Li, J. R. Li, Y. N. Han, J. Li and L. L. Song, *ACS Sustainable Chem. Eng.*, 2022, **10**, 13254–13265.
44 Y. Q. Zhou, Y. N. Liang, X. N. Liu and X. H. Qi, *ACS Sustainable Chem. Eng.*, 2023, **11**, 12052–12064.
45 A. A. Ansari, A. K. Parchur and G. Y. Chen, *Coord. Chem. Rev.*, 2022, **457**, 214423.
46 K. Y. Zhang, S. T. Song, S. Huang, L. Yang, X. C. Wu, F. Lu and J. J. Zhu, *Small*, 2018, **14**, 1802292.
47 K. Y. Zhang, L. Yang, F. Lu, X. C. Wu and J. J. Zhu, *Small*, 2018, **14**, 1703858.
48 S. N. Deepti and P. S. Nagaraj, *Sens. Actuators, B*, 2016, **230**, 140–148.
49 X. D. Tang, H. Y. Wang, H. M. Yu, B. Bui, W. Zhang, S. Y. Wang, M. L. Chen, L. Q. Yuan, Z. Z. Hu and W. Chen, *Mater. Today Phys.*, 2022, **22**, 100576.
50 D. Kuzmanović, D. M. Stanković, D. Manojlović, K. Kalcher and G. Roglić, *Diamond Relat. Mater.*, 2015, **58**, 35–39.